TU Delft

Delft University of Technology

Correlation between Lidar measured wind speeds and aerodynamic loading

Giyanani, A.; Savenije, F. J.; Van Bussel, G. J.W.

DOI
10.1088/1742-6596/1037/5/052038

Publication date
2018

Document Version
Final published version

Published in
Journal of Physics: Conference Series

Citation (APA)
Giyanani, A., Savenije, F. J., & Van Bussel, G. J. W. (2018). Correlation between Lidar measured wind speeds and aerodynamic loading. *Journal of Physics: Conference Series*, *1037*(5), Article 052038. https://doi.org/10.1088/1742-6596/1037/5/052038

Important note
To cite this publication, please use the final published version (if applicable).
Please check the document version above.

Copyright
Other than for strictly personal use, it is not permitted to download, forward or distribute the text or part of it, without the consent of the author(s) and/or copyright holder(s), unless the work is under an open content license such as Creative Commons.

Takedown policy
Please contact us and provide details if you believe this document breaches copyrights.
We will remove access to the work immediately and investigate your claim.

This work is downloaded from Delft University of Technology.
For technical reasons the number of authors shown on this cover page is limited to a maximum of 10.

Journal of Physics: Conference Series

PAPER • **OPEN ACCESS**

Correlation between Lidar measured wind speeds and aerodynamic loading

To cite this article: A Giyanani *et al* 2018 *J. Phys.: Conf. Ser.* **1037** 052038

View the article online for updates and enhancements.

Related content

- IR differential-absorption lidars for ecological monitoring of the environment
B I Vasil'ev and Oussama Mannoun
- Wind shear proportional errors in the horizontal wind speed sensed by focused, range gated lidars
P Lindelöw, M Courtney, R Parmentier et al.
- Investigation of the Impact of the Upstream Induction Zone on LIDAR Measurement Accuracy for Wind Turbine Control Applications using Large-Eddy Simulation
Eric Simley, Lucy Y Pao, Pieter Gebraad et al.

IOP ebooks™

Bringing you innovative digital publishing with leading voices to create your essential collection of books in STEM research.

Start exploring the collection - download the first chapter of every title for free.

This content was downloaded from IP address 131.180.130.242 on 16/07/2018 at 11:06

IOP Conf. Series: Journal of Physics: Conf. Series **1037** (2018) 052038 doi:10.1088/1742-6596/1037/5/052038

Correlation between Lidar measured wind speeds and aerodynamic loading

A Giyanani[1], F J Savenije[2] G J W van Bussel[1]

[1] Delft University of Technology (TU Delft), Wind Energy Research Group, Aerospace Engineering faculty, Kluyverweg 1, 2629HS Delft, The Netherlands
[2] Energy Research Centre of the Netherlands (ECN), Westerduinweg 3, 1755 LE Petten

E-mail: ashimgiyanani@gmail.com

Abstract.

The IEC standards prescribe an inflow wind field based on models with empirical assumptions to perform load calculations. The use of preview wind speed measurements using nacelle-mounted Lidars allows mitigation of structural loads by suggesting appropriate control action. This relationship is affected by uncertainty in site conditions and the dynamic control of wind turbine in different operation regimes. Although efforts have been put to derive the relation between the aerodynamic loading and the wind speed, there is scope to explore this relation using measurements. Deriving the load statistics based on the inflow wind field is therefore necessary to establish the correct control strategies. This study focuses on two aspects: firstly, the effect of variability in the inflow conditions due to wind speed fluctuations, turbulence and wind evolution on loading statistics and secondly, the effect of different wind turbine operation modes and Lidar measurement ranges on loading statistics. By understanding the effect of these two aspects on aerodynamic loading, a suitable control strategy can be designed by establishing correlation and coherence based look-up tables with inflow-loading relationship for each operation regime. The study defines a correlation between the Lidar measured wind speed and aerodynamic loading for three Lidar measurement ranges at below and above rated operation modes. Strong correlations are observed at above-rated operation, while uneven correlations at below-rated operation are observed. Strong correlations are observed for turbulence intensities higher than 12%. The preview distances of 50 m and 110 m provide the high correlation estimates The study of coherence between these two signals provides useful insights on the evolution of wind, the length scales present and the frequencies. The coherence remains high for wavelengths upto 200 m for above-rated and below-rated operations, the time scale was found to be around 2-2.5 s and the decay parameter ranges from 2 to 7.

1. Introduction

The IEC-61400-1 standard specifies the design classes associated with the site conditions, related to annual average wind speeds, gust occurrences and turbulence statistics at a site [1]. The wind turbine design shall conform to these site conditions to be certified for commercial purposes. Since, the load simulations under existing site conditions provides the expected dynamic loading behaviour without any uncertainty limits, additional experimental wind and loading measurements are needed to narrow the knowledge gap and verify the simulated results. By defining the correlation statistics based on site conditions and turbine specific loading response, the turbine response for real-time inflow measurements can be predicted in advance.

In this study, the inter-relationship between the inflow conditions and aerodynamic loading is analysed using correlation functions, spectral responses and coherence functions. The inflow wind speed measured by Lidar at different ranges is tested to provide the optimal distance for correlation studies. The effect of inflow wind on the aerodynamic loading is analysed using

Content from this work may be used under the terms of the Creative Commons Attribution 3.0 licence. Any further distribution of this work must maintain attribution to the author(s) and the title of the work, journal citation and DOI.
Published under licence by IOP Publishing Ltd

aerodynamic torque estimates and blade out-of-plane bending moment measurements at below and above rated operation modes.

The aerodynamic torque contains contributions from blade geometry, blade pitch angle and rotor speed and is well suited for this study. Most wind turbines follow the maximum power-point tracking control strategy, where the tip speed ratio λ and aerodynamic torque Q are maintained at an optimum level to maximise power extraction. Q is related to the wind speed U_r using the relation Eq. (1); where the torque coefficient C_Q is mainly dependent on λ and pitch angle β and relates to the power coefficient C_P using C_Q=C_P/λ, ρ is the air density and R_r is the rotor radius.

$$Q = \frac{1}{2}\rho\pi {R_r}^3 {\bar{U}_r}^2 C_Q(\lambda, \beta) \tag{1}$$

Fig. 1a shows the Torque and rotor speed versus wind speed curve used for maximum power point tracking. The wind turbine operational regime is divided into different ranges. The blades are pitched to extract maximum aerodynamic efficiency at idle operation ($\bar{U}$<4 m/s). Following the maximum power tracking strategy, the bladed are pitched at nominal to derive maximum power from the wind at below-rated operation (4 m/s<$\bar{U}$<12 m/s). At around 12 m/s, the pitch is adjusted to provide a smooth transition into the rated operation (12 m/s<$\bar{U}$<25 m/s). At above rated operation, the pitch-to-vane strategy is followed to keep the torque, rotational speed and power at constant optimum levels, while keeping the loads low. A measured torque-wind speed curve for the complete operating range is illustrated in Fig. 1b. The high scatter in the Q–U_r curve emerges as the derived estimates of Q and U_r are sampled at 64 Hz using ECN's wind estimator. A short description of the measurement setup and the methodology to define the relationship between aerodynamic loading and inflow wind is given in the next section.

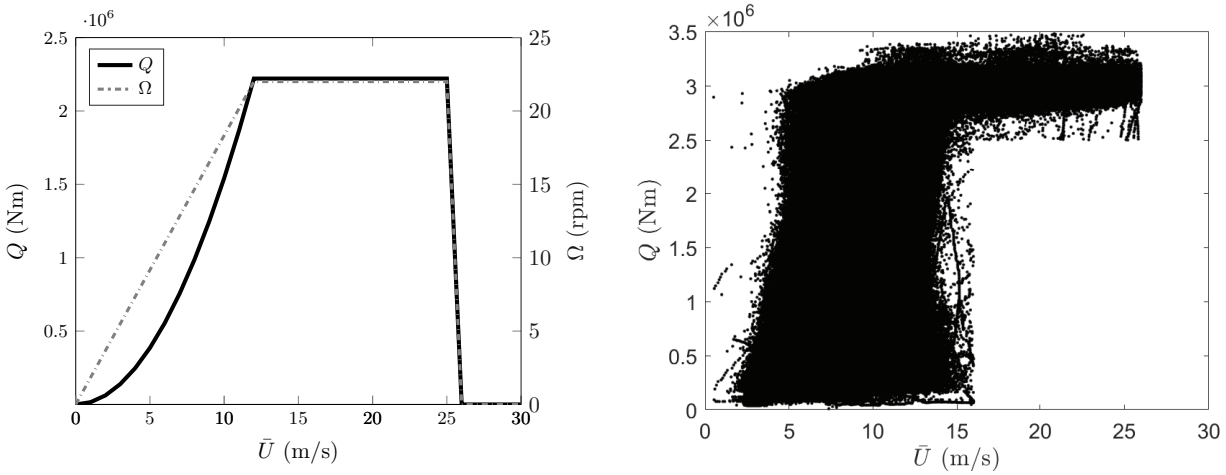

(a) General torque speed curve of a wind turbine [2] (b) Measured torque wind speed curve

Fig. 1: General torque and RPM curve as a function of wind speed

2. Methodology

2.1. Measurement setup

The experimental setup consists of an Avent Lidar installed on a Darwind XD-115 wind turbine with a hub height of 100 m at ECN's wind turbine test site in Wieringermeer. This site with flat terrain and distant houses along with some rows of trees approximates to z_0=0.1 m. The five beam pulsed Lidar is oriented with a central beam and four other beams at a cone angle of 15° as seen in Fig. (2). The sampling frequency for Lidar wind measurement is 4 Hz for each beam with 10 equidistant measurement ranges from 50 m to 185 m, in front of the wind turbine. The wind field is assumed to be homogeneous, with irrotational flow, no shear and no veer conditions. The effects of vertical shear and horizontal veer are reduced considerably

by averaging the wind measurements from the 5 beams at each Lidar distance. Additionally, the range weighting function spatially averages the wind speed along the length of the beams. As the wind is also spatially filtered along the blades when the rotor generates aerodynamic torque, the spatial and temporal averaging of the Lidar wind speeds is assumed to be a good estimate of rotor equivalent wind speed [3]. For the correlation study, three measurement ranges x=50, 110, 170 m are considered, while the coherence study is performed with x=50 m only. The loading measurements i.e. aerodynamic torque, blade in-plane and out-of-plane bending moment and estimated undisturbed wind speed were initially sampled at 64 Hz, but are later resampled to 4 Hz for correlation study comparison.

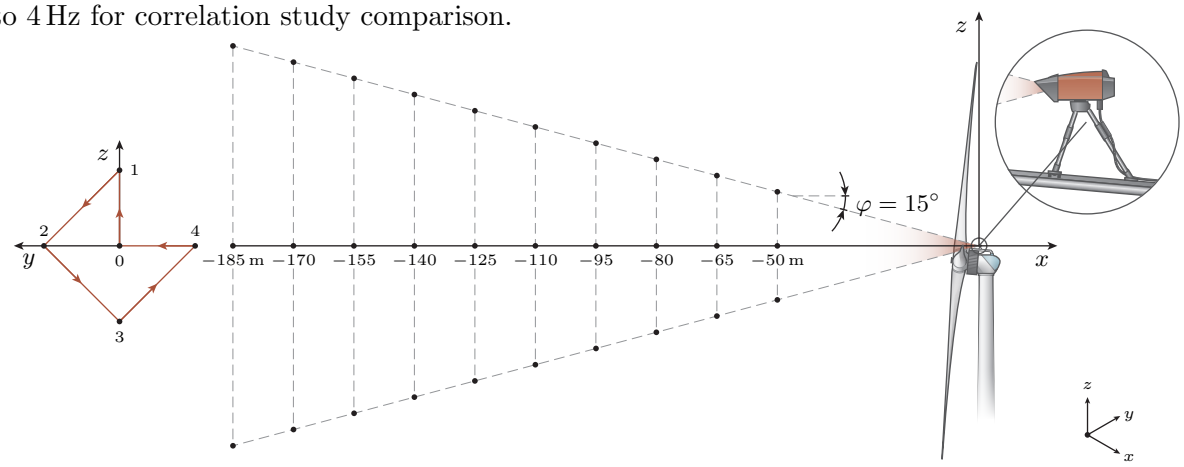

Fig. 2: Pulsed Lidar mounted on the nacelle of Darwind XD115-5MW wind turbine [5]

The time series from the Lidar and aerodynamic loading are post-processed for any spikes, anomalies (e.g. 0.5 m/s < $\bar{U}$ < 35 m/s) and low quality data(e.g. low CNR values i.e. −17 dB > CNR > 0 dB), low Lidar availability i.e. (< 75%) [4]. The aerodynamic loading measurements are low-pass filtered and resampled to 4 Hz, to match the sampling frequency of the Lidar wind measurements. Six months of data is selected for this study over a period 01/11/2013 to 30/04/2014 amounting to N=19771200 samples. The time series are further segmented into operation modes with a minimum segment width of 75 s in order to achieve statistical significance for the tests performed, especially in cases of coherence and power spectral densities. The small gaps due to filtering or measurement errors are interpolated using a cubic spline.

2.2. Correlation of Lidar measured wind speed with loads

The cross-correlation ρ_{uy} is carried out on a moving window of 300 data points with 50% overlaps sampled at 4 Hz over a time period of T=75 s. By determining the location of the correlation peak, the time delay τ between the wind speed $u(t)$ and the aerodynamic loading $y(t)$ can be determined [6, refer p. 549-554 on correlation]. The correlation-wind speed curves illustrated in Figs. 3a and 3b are compared between the $U(x$=50$m)$ and aerodynamic loading, Q and M_{oop} respectively. Higher correlations are achieved in the below-rated operation mode for both Q and M_{oop}. However, the scatter in ρ_{uy} is large throughout with very few points beyond the 16 m/s and very low correlations around rated wind speed. Some methods to optimise the correlations e.g. moving window of 1200 points and an appropriate filter will be implemented in the future. The central mark in the box defines the median of that respective bin, the box edges indicate the 25 and 75 percentiles and the whisker edges indicate the minimum and maximum excluding the outliers.

The time delay consists of two parts, one due to the distance that the wind needs to convect from the lidar measurement plane towards the wind turbine and the other due to dynamic inflow conditions especially at above-rated conditions due to pitch activation resulting in induced velocity changes at the rotor. In this study, the time delay due to convection and wind

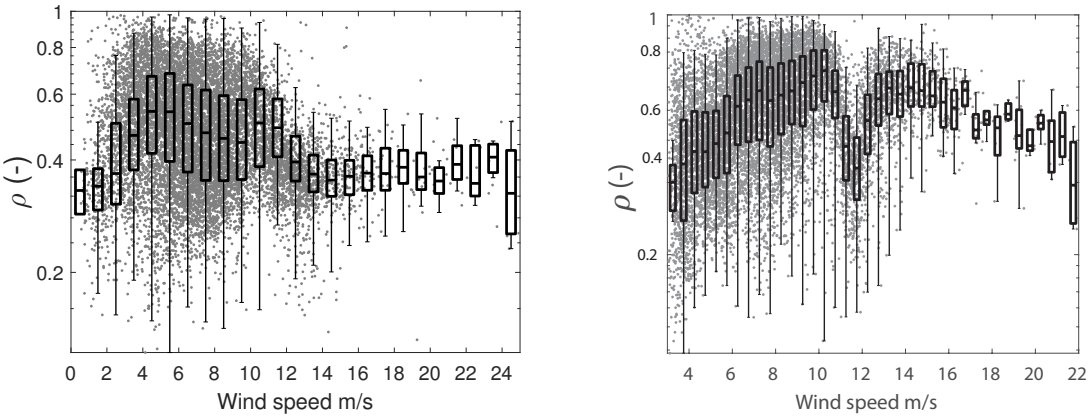

(a) Aerodynamic torque response Q (b) Blade out-of-plane bending moment M_{oop}

Fig. 3: Correlation between aerodynamic loading (Q & M_{oop}) and wind speed

evolution are considered and the dynamic inflow condition is avoided as the dynamic inflow is an extensive topic on it's own. The induced velocity and the time delay due to dynamic changes in aerodynamic loading are affected significantly at distances lower than 50 m in front of the turbine and at very short time constants making the current analysis setup unsuitable for the dynamic inflow study.

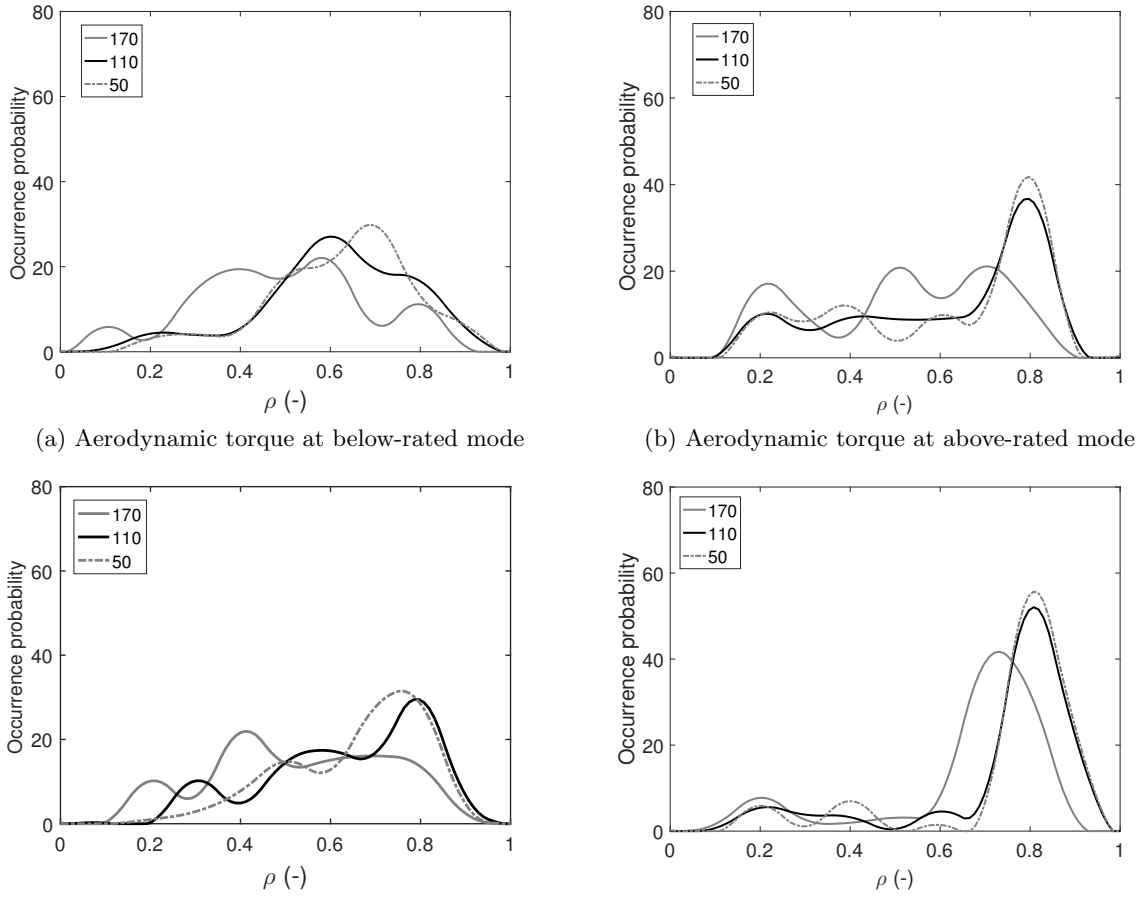

(a) Aerodynamic torque at below-rated mode (b) Aerodynamic torque at above-rated mode

(c) Out-of-plane bending moment at below-rated mode (d) Out-of-plane bending moment at above-rated mode

Fig. 4: Effect of Lidar range on correlation between Q-U_r and M_{oop}-Ur using smoothed histograms

In order to determine if the correlation studies are affected by the distance of Lidar measurement plane or if the assumption of Taylor's frozen turbulence is suitable, additional classification of the correlation and time delay studies are performed for three Lidar measurement ranges at x=170 m (undisturbed wind speed), x=110 m (Lidar focal point, most accurate) and x=50 m (closest measurement to wind turbine). The assumption of undisturbed wind speed existing at 170 m is based on the fact that at around x=1.5 D from the turbine, the induction factors are less than 5% [7] [3]. The occurrence probabilities for correlation bins of 0.05 are shown separately for below-rated and above-rated operation in Fig. (4) for Q and M_{oop}. Higher correlations are observed at above-rated operation for $U(x$=50m, 110m), while no specific trends are observed at below-rated operation.

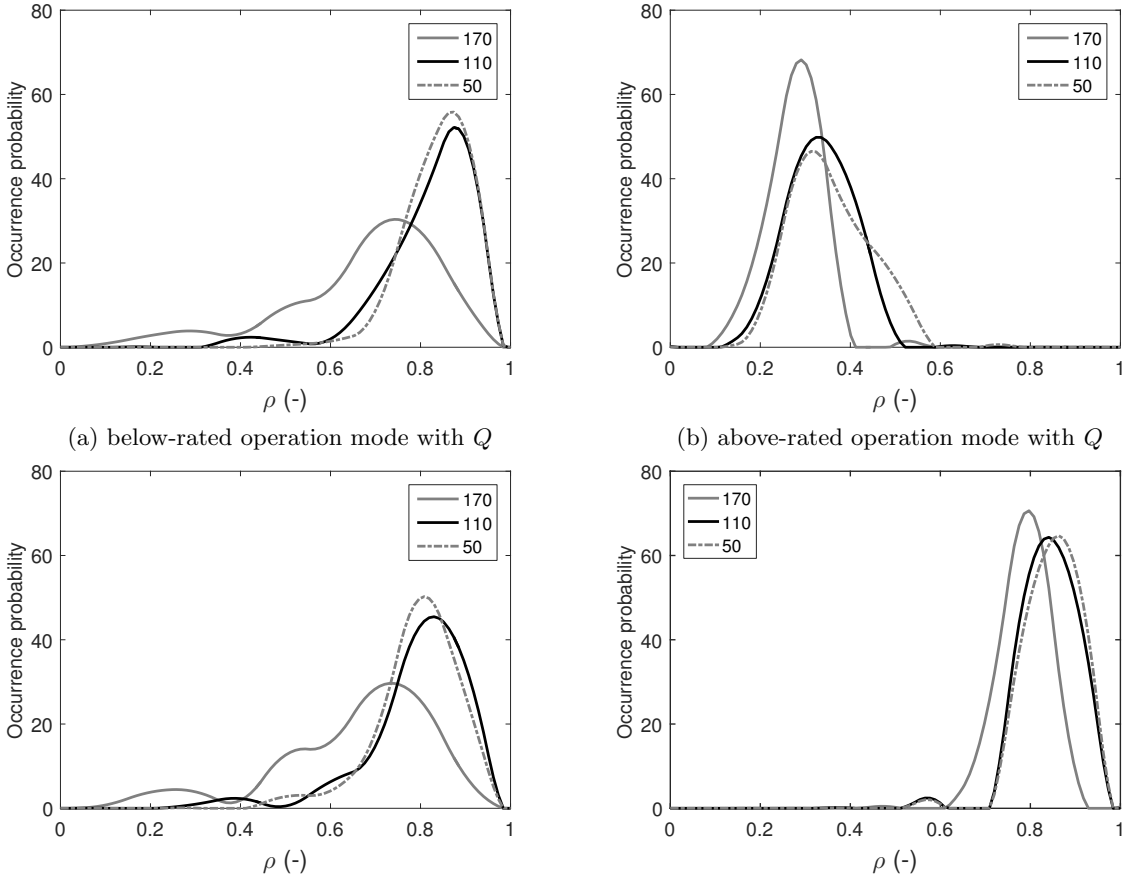

(a) below-rated operation mode with Q

(b) above-rated operation mode with Q

(c) below-rated operation mode with M_{oop}

(d) above-rated operation mode with M_{oop}

Fig. 5: Effect of Lidar ranges on correlation between Q–U_r and M_{oop}–U_r at high I using smoothed histograms

The relationships between the load fluctuations and the bending moments with respect to the fluctuations in wind are often assumed to be linear [8]. As the relation between the wind and loads is non-linear as seen in Fig. (1) and as the low correlation values at below-rated operation shown in Figs. 4a and 4c might be linked to high variation of turbulence intensity, the effect of higher turbulence intensity i.e. I>0.12 on the aerodynamic loading becomes an important aspect to be validated. The turbulence intensity $I=\sigma/\bar{U}_r$ is defined using the standard deviation σ and mean $\bar{U}_r$ of the wind speed over a moving window of 300 data points with 50% overlaps sampled at 4 Hz i.e. T=75 s. High correlation coefficients were observed at below-rated operation for both Q and M_{oop} for $U(x$=50m, 110m). The surprising result in Fig. 5b, might be associated to robust controlling of the wind turbine based on $U(x$=170) m at above-operation with high turbulence

conditions. The adjustment of the pitch angle to maintain constant rotor speed irrespective of rising wind speed is assumed to cause the low correlation peaks observed at $\rho \approx 0.3$

2.3. Coherence estimation

The wind speed measurements $u(t)$ at x=50 m are and the aerodynamic loading $y(t)$, seperated over a distance of Δx=50 m in space are considered for spectral and coherence estimation. The spectral density estimates $S_{uy}(f)$ defined over frequency f are performed using Welch spectral estimator for $N_s \approx 600$ segments based on continuous segments with N_{fft}=4096, which are subdivided into $m \approx 8$ subsegments with a width of 300 points and 50% overlaps. These subsegments are then averaged to obtain N_s averaged Power spectral density estimates in order to reduce the bias and variance as suggested by [9] [10].

$$S_{uy}(f) = \frac{1}{T}\int_{-T}^{T} R_{uy}(\tau)e^{-2\pi i f\tau}d\tau \tag{2}$$

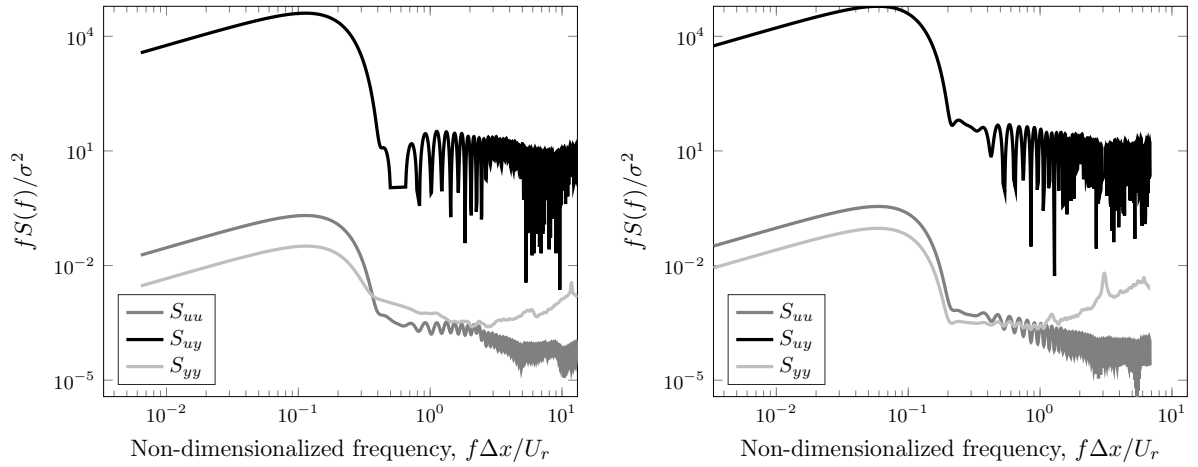

(a) PSDs for below rated operation with Q

(b) PSDs for above rated operation with Q

(c) PSDs for below rated operation with M_{oop}

(d) PSDs for above rated operation with M_{oop}

Fig. 6: Cross-spectral PSD's and Autopower PSD's for wind speed and aerodynamic loading

The cross-spectral density was normalized and scaled using a Hamming window $H(m)$ of length m given by Eq. (3), where K is the scaling function, F_s is the sampling frequency, N_m is the number of windows and $H^*(m)$ indicates the complex conjugate of $H(m)$. The signal power

was transferred to positive frequency one-sided spectrum i.e. 0 to nyquist frequency F_n=2 Hz.

$$S_{uy} = S_{uy}/K_u;\ \text{where, } K = \frac{kF_s}{N_m}\sum_{i=0}^{N_m-1} < H(m)H^*(m) > \tag{3}$$

The magnitude squared coherence γ^2_{uy} is calculated from the normalized cross-spectral density functions according to Eq. (4). It ranges from 0 and 1, where γ^2_{uy}=1 indicates strong similarity in the spectral densities at given frequencies and γ^2_{uy}=0 indicates that the two signals are independent random signals. The coherence function measures the variation in energy content of two stationary random signals between two points in space over a range of frequency. For longitudinal separations, Davenport proposed an exponential decay of the coherence of the form Eq. (4) [11]. The value of $\hat{\alpha}$ is estimated by optimising the least square error estimate to the minumum for the function $J(\alpha)$ as shown in Eq. (5) [3].

$$\gamma^2_{uy}(x,x',f) = \frac{|S_{uy}(x,x',f)|^2}{S_{uu}(x,f)S_{yy}(x',f)} = exp(-\frac{\alpha f}{\bar{U_r}}) \tag{4}$$

$$\hat{\alpha} = min\{J(\alpha)\} = \frac{1}{\int_0^{f_n} S_{uu}(f)}\sum_{i=1}^{N}\int_0^{f_n} S_{uu}(f)\left(\gamma^2_{uy}(x,x',f) - exp(-\frac{\alpha\sigma_{uu}f_{uy}\Delta x}{\bar{U_r}^2}\right) \tag{5}$$

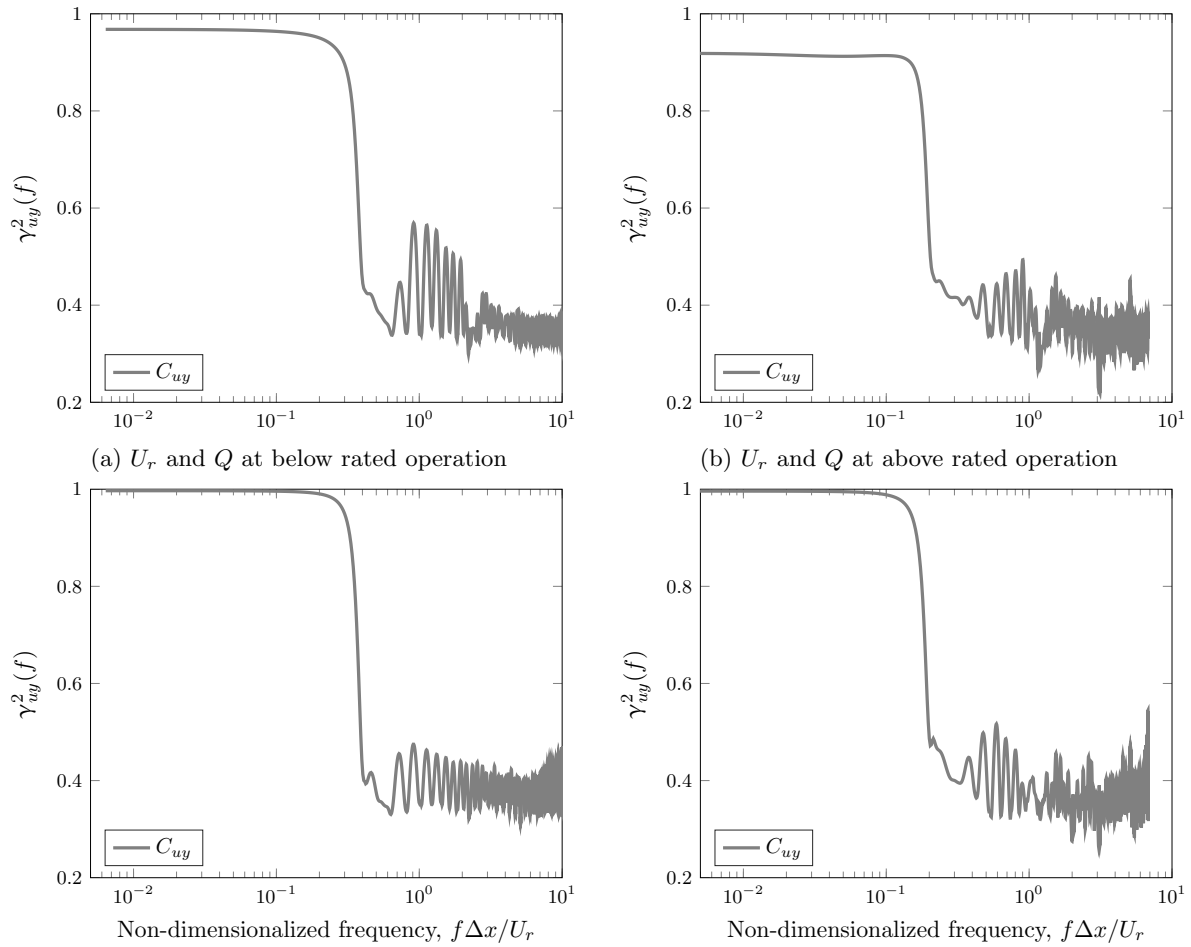

(a) U_r and Q at below rated operation

(b) U_r and Q at above rated operation

(c) U_r and M_{oop} at below rated operation

(d) U_r and M_{oop} at above rated operation

Fig. 7: Magnitude squared coherence between aerodynamic loading and wind speed

The correlation coefficient ρ and coherence decay parameter α are greatly affected by integral length scales of the turbulence present in the wind at a site. The length scale ${}^{x}L_u$ is the measure of the average eddy size in the longitudinal direction and is dependent on the variation of the wind speed ${\sigma^2}_u$, surface roughness z_0 and hub height H.

The integral time scale is the time over which the fluctuations in the wind speed are correlated with each other. The Lidar measurement at x=50 m and the wind speed at x=0 m estimated by the ECN wind estimator are used for the autocorrelation function [2]. By integrating the autocorrelation function from zero lag to the first zero-crossing as given in Eq. (6), the integral time scale was calculated. Finally, the integral length scale ${}^{x}L_u$ was calculated from the integral time scale T_i assuming Taylor's frozen turbulence hypothesis according to ${}^{x}L_u$=$\mathtt{T}_i\bar{U}_r$ [12][6].

$$T_i = \int_0^{t_0} \rho_{uu}\tau d\tau \tag{6}$$

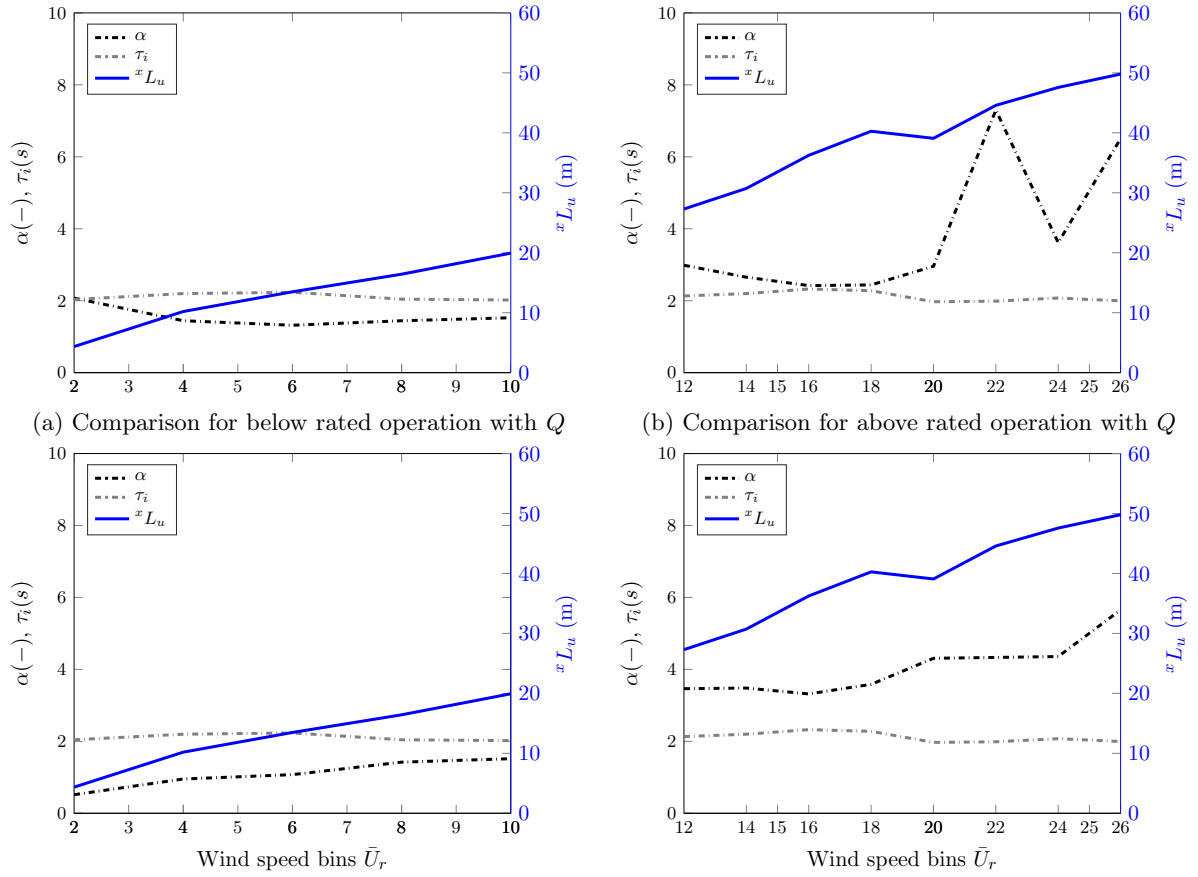

(a) Comparison for below rated operation with Q

(b) Comparison for above rated operation with Q

(c) Comparison for below rated operation with M_{oop}

(d) Comparison for above rated operation with M_{oop}

Fig. 8: Time delay, decay coefficient and the integral length scale for the whole sample range binned according to wind speeds

3. Results and Discussion

The correlation curves established in Section 2.2 are an attempt to replicate the torque-speed curves and the thrust-speed curves used in wind energy to define the relationship between the power, thrust and torque to the wind speed. The correlation coefficient was used to understand the relationship between critical aerodynamic loading parameters and inflow wind measurements.

It is clear from Figs. 4b and 4d that the aerodynamic loading is strongly correlated with the wind speed measurements at above-rated operation mode; while weak and uneven correlations are observed at below-rated operation, see Figs. 4a and 4c. In order to explain these differences, the inflow parameters like the length scale ${}^{x}L_u$ and the effect of turbulence intensity I_u on the

correlation are examined. The ${}^{x}L_u$ present in the wind at below-rated operation passing through the two points x=50 m and x=0m (rotor plane) are of the order of upto 20m as shown in Figs. 8a and 8c. In cases where the I_u exceeded 0.12, the correlation between the aerodynamic loading and the I_u at below-rated operation was strongly correlated as shown in Figs. 5a and 5c.

The Lidar range gates were tested for their suitability for the correlation study. The measurement distances of x=110 m and x=50 m consistently provided high correlation estimates between the measured wind and aerodynamic loading. There was very little difference in the performance between these two measurement distances and both are recommended for Lidar-assisted control of the wind turbines. The wind speed measurements measured at x=170 m shown in Figs. 4d, 5a and 5c provide low correlations due to incoherent structures and wind evolution. The highest occurrence probabilities for ρ_{uy} and τ_{uy} per bin for Q and M_{oop} at below and above-rated operation are given in the Tab. (1). As expected, the time delay τ_{uy} increases as the distance from the turbine increases. Assuming Taylor's frozen turbulence hypothesis, a rough estimate of the rotor effective wind speed can be made based on τ_{uy} and Δx.

The spectra in Fig. (6) illustrate the amount of energy present in the signal as a function of frequency. By analysing the spectra, it is important to determine the rotor rotation frequency (1P) and the blade-passing frequency (3P) for a three-bladed wind turbine. The spectra in Figs. 6c and 6d clearly display the 1P, 2P and 3P frequencies for M_{oop}, whereas the excitation frequencies for the Q are hardly recognisable. The combined spectrum S_{uy} includes the turbulent nature of the wind spectrum (S_{uu}) and the peaks of the loading spectrum (S_{yy}), where the amplitude is enhanced at excitation frequencies. A difference in the excitation frequencies at below-rated and above-rated operation was observed for M_{oop} and Q, e.g. at below-rated operation, the excitation frequency was observed at around $1P$=1.25 (-) as shown in Fig. 6c and $1P$=1 (-) at above-rated operation as shown in Fig. 6d are found. A less sharp peak is observed at below-rated excitation frequency as the rotor speed is not constant. These differences in excitation frequencies shall be considered while designing the control strategy for different operation modes of the wind turbine.

Tab. 1: Occurrence probabilities for ρ and τ for Q at below and above-rated wind speeds

Aerodynamic Torque, Q								
	Below rated operation mode				Above rated operation mode			
Range (m)	ρ (-)	P(ρ) (%)	τ (s)	P(τ) (%)	ρ (-)	P(ρ) (%)	τ (s)	P(τ) (%)
170	0.6-0.65	22%	21-22	45%	0.7 - 0.75	20%	13 - 14	59%
110	0.6-0.65	27%	14-15	65%	0.8 - 0.85	37%	10 -11	57%
50	0.7-0.75	30%	8-9	50%	0.8 - 0.85	40%	6 - 7	60%
Out-of-plane bending moment, M_{oop}								
170	0.4-0.45	22%	21-22	32%	0.7-0.75	42%	12-12.5	68%
110	0.8-0.85	30%	13-14	53%	0.8-0.85	52%	9-9.5	63%
50	0.75-0.8	32%	7-8	75%	0.8-0.85	56%	5-5.5	66%

The coherence plots for M_{oop} and Q drop at the same frequency level for a given operation mode. The coherence drops below 0.4 at $f\Delta x/U_r$=0.25=0.04 Hz for below rated operation and $f\Delta x/U_r$=0.2=0.056 Hz for above rated operation, where Δx=50 m and U_r=8 m/s and U_r=14 m/s respectively. The coherence thus remains high for wavelengths of the order of λ=U_r/f=200 m for below rated operation and λ=250 m for above rated operations for the given site. Veldkamp achieved length scales of the same length when using Kaimal spectrum for longitudinal fluctuations for three different locations [13]. The high coherence at lower frequencies are related to large eddies and as the length scale decreases, the decay parameter α increases. When performing further analysis as shown in Fig. (8), the time scale of turbulence was found

to be consistent between 2-2.5 s throughout the wind speed range and operation, while the decay parameter ranges from 2 to 7. The low number of data points in the bins at $U_r = 22\,\mathrm{m/s}, 24\,\mathrm{m/s}$ are responsible for the high fluctuations in α, see 8b. The integral length scale and the decay parameter increase with an increase in U_r as can be seen from Fig. 8d.

4. Conclusions and further work

The objective of this study was to determine the inter-relationship between the aerodynamic loading and the inflow wind speed. The conclusions for this study are as follows

- The correlation curves can be used as lookup tables for Lidar-assisted control, with the focus to reduce aerodynamic loading. The length of the moving window and filtering properties need to be optimised further to improve the estimates.
- The wind speed and aerodynamic loading are strongly correlated at above-rated operation. The weak correlation at below-rated operation is associated with smaller length scales and high variance in the turbulence intensity I>0.12.
- The Lidar ranges from x=50 m to x=110 m are most suitable for Lidar-assisted control.
- The coherence function remains high upto f=0.04 Hz i.e. for wavelengths of the order of λ=200 m at below-rated operation and upto f=0.056 Hz i.e. for wavelengths of the order of λ=250 m at above-rated operation.

For future work, the effect of shear and atmospheric stability on the correlation and coherence would be considered. The damage potential in wind according to [5] will be validated and the coherence decay from one range gate to the other will be considered.

Acknowledgments

This work was carried within the LAWINE project, funded by TKI Wind-op-Zee. The project partners ECN, XEMC Darwind BV and Avent-Lidar Technology are hereby acknowledged for their contributions. Thanks to Dr.ir.W.Bierbooms, G.Bergman, R.Bos and M.Boquet for their support during meetings and discussions.

References

[1] IEC, "IEC 61400-1 Ed.3 Wind turbines - Design requirements." 2010.
[2] E. van der Hooft, P. Schaak, and T. van Engelen, "Wind turbine control algorithms," no. December, 2003.
[3] E. Simley, L. L. Y. Pao, P. Gebraad, and M. Churchfield, "Investigation of the Impact of the Upstream Induction Zone on LIDAR Measurement Accuracy for Wind Turbine Control Applications using Large-Eddy Simulation," *Journal of Physics: Conference Series*, vol. 524, p. 012003, jun 2014.
[4] A. Giyanani, W. Bierbooms, and G. van Bussel, "Lidar uncertainty and beam averaging correction," *Advances in Science and Research*, vol. 12, no. April, pp. 1–5, 2015.
[5] R. Bos, A. Giyanani, and W. Bierbooms, "Assessing the Severity of Wind Gusts with Lidar," *MDPI Remote Sensing of Wind Energy*, vol. 8, no. 9, p. 758, 2016.
[6] I. M. Cohen, P. K. Kundu, and D. R. Dowling, *Fluid Mechanics*. Elsevier Inc., 5th ed., 2012.
[7] D. Medici, S. Ivanell, J. Dahlberg, and P. H. Alfredsson, "The upstream flow of a wind turbine : blockage effect," *Wind Energy*, vol. 17, no. January, pp. 691–697, 2011.
[8] L. S. Kelley N D; Jonkman, B J; Bialasiewicz, J T; Scott, G N; Redmond, "The Impact of Coherent Turbulence on Wind Turbine Aeroelastic Response and Its Simulation," *American Wind Energy Association WindPower 2005 Conference and Exhibition*, p. 17, 2005.
[9] E. Cheynet, J. B. Jakobsen, B. Svardal, J. Reuder, and V. Kumer, "Wind Coherence Measurement by a Single Pulsed Doppler Wind Lidar," *Energy Procedia*, vol. 94, no. 1876, pp. 462–477, 2016.
[10] K. Saranyasoontorn, L. Manuel, and P. S. Veers, "A Comparison of Standard Coherence Models for Inflow Turbulence With Estimates from Field Measurements," *Journal of Solar Energy Engineering*, vol. 126, no. 4, p. 1069, 2004.
[11] A. G. Davenport, "The spectrum of horizontal gustiness near the ground in high winds," *Quarterly Journal of the Royal Meteorological Society*, vol. 87, no. 372, pp. 194–211, 1961.
[12] G. Taylor, "The spectrum of turbulence," *Proceedings of the Royal Society of London, Series A, Mathematical and Physical Sciences*, vol. 164, no. Feb,18, 1938, pp. 476–490, 1938.
[13] D. Veldkamp, *Chances in Wind Energy A Probabilistic Approach to Wind Turbine Fatigue Design*. No. 1, Delft, The Netherlands: DUWIND Delft University Wind Energy Research Institute, 2006.